Results in Optics 21 (2025) 100847

Contents lists available at ScienceDirect

Results in Optics

journal homepage: www.elsevier.com/locate/rio

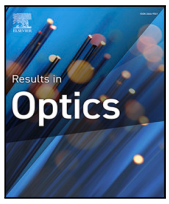

Optical emulation of quantum state tomography and Bell test—A novel undergraduate experiment

Eden Arbel [a,1], Noa Israel [a,1], Michal Belgorodsky [a,1], Yonathan Shafrir [a,1], Alona Maslennikov [b], Sara P. Gandelman [a], Georgi Gary Rozenman [a,c,d,*]

[a] Raymond and Beverly Sackler School of Physics & Astronomy, Faculty of Exact Sciences, Tel Aviv University, Tel Aviv 69978, Israel
[b] School of Chemistry, Raymond and Beverly Sackler Faculty of Exact Sciences and Tel Aviv University Center for Light-Matter Interaction, Tel Aviv University, Tel Aviv 6997801, Israel
[c] School of Electrical Engineering, Iby and Aladar Fleischman Faculty of Engineering, Tel Aviv University, Tel Aviv 69978, Israel
[d] Department of Mathematics, Massachusetts Institute of Technology, Cambridge, MA 02139, USA

ARTICLE INFO

Keywords:
Bell test
Quantum state tomography
Quantum cryptography
Quantum Optics

ABSTRACT

This paper presents an innovative experiment and theoretical framework designed for senior-level undergraduate students to explore quantum state tomography and Bell inequality tests. The experiment utilizes pulsed laser light and a carefully engineered optical system to emulate quantum entanglement, enabling students to investigate foundational quantum phenomena using accessible laboratory tools. Through practical measurements and simulations, students reconstruct quantum states and analyze correlations indicative of entanglement and non-locality. The setup includes polarization analysis across multiple measurement bases and culminates in the measurement of Bell's parameter using the CHSH test. By combining experimental emulation with computational analysis, this approach provides a compelling educational bridge between abstract quantum theory and hands-on experiments, highlighting the conceptual and practical relevance of quantum entanglement in modern physics.

1. Introduction

Entanglement and quantum state tomography represent two of the most captivating and foundational elements of quantum mechanics, illustrating its stark contrast with the classical understanding of the physical world (Scully and Suhail Zubairy, 1999). Entanglement, famously introduced through the Einstein–Podolsky–Rosen (EPR) thought experiment, reveals a strikingly non-classical phenomenon where the states of particles become so strongly correlated that they can no longer be described independently, even when separated by large distances (Einstein et al., 1935). This inseparability leads to notable phenomena, such as the strong polarization correlations observed between entangled photons, challenging the classical concept of locality (Doplicher, 2010). According to the Copenhagen interpretation, these correlations arise from the inherently non-local nature of quantum measurements, where measuring one particle instantaneously affects the state of its entangled partner, regardless of the distance between them. Bell's inequality explores this distinction further by contrasting the predictions of quantum mechanics with those of local realism, providing a framework to test these competing views. Repeated experiments have consistently upheld the predictions of quantum mechanics, solidifying its non-local interpretation (Sulimany et al., 2024; Lib et al., 2022).

Beyond the intriguing phenomenon of entanglement, quantum state tomography serves as a powerful tool for fully characterizing the quantum state of a system (Gebhart et al., 2023). By reconstructing the state from experimental measurements, this technique allows researchers to not only confirm the presence of entanglement but also to precisely assess its quality. For instance, in quantum computing, quantum state tomography is indispensable for verifying the accuracy of qubits in superposition states or entangled pairs, ensuring that the computations remain robust (Stricker et al., 2022). Similarly, in quantum communication protocols, such as quantum key distribution, tomography is essential for certifying the integrity of the entangled photon pairs that form the foundation of secure transmission (Kundu et al., 2023b).

An exciting example comes from experiments with multi-photon entanglement, where quantum state tomography has been used to reconstruct the density matrices of large entangled systems, enabling breakthroughs in quantum information processing (Rey-de Castro et al.,

* Corresponding author at: Department of Mathematics, Massachusetts Institute of Technology, Cambridge, MA 02139, USA.
E-mail address: garyrozenman@protonmail.com (G.G. Rozenman).
[1] Equal contribution.

https://doi.org/10.1016/j.rio.2025.100847
Received 10 February 2025; Received in revised form 19 April 2025; Accepted 7 June 2025
Available online 1 July 2025

2013). For instance, photons occupying multiple spatial modes generated via spontaneous four-wave mixing in a few-mode fiber have been shown to hold great promise for high-dimensional quantum communication, paving the way for advanced quantum protocols using standard fiber technologies (Sulimany and Bromberg, 2022).

Recently, there have been exciting developments in more efficient and scalable quantum tomography techniques, which allow for the characterization of even larger and more complex quantum systems (Wang et al., 2020). This technique is also fundamental in testing foundational aspects of quantum theory, such as Bell's theorem, by providing a clear view into the statistical properties of quantum states (Nadlinger et al., 2022).

The density matrix revealed through tomography encapsulates all of a quantum system's statistical characteristics, including coherence and decoherence effects, making it a vital component not just in fundamental physics but also in practical applications like quantum error correction and fault-tolerant quantum computing (Rozenman et al., 2023c). By unlocking these insights, quantum state tomography plays a critical role in advancing technologies at the forefront of the quantum revolution (Liu et al., 2022).

Recent advancements in laser technology have significantly enhanced the accessibility of quantum experiments, particularly in educational settings (Bloom et al., 2022; Paraïso et al., 2021; Pospiech, 2021; Parakh et al., 2020; Gandelman et al., 2025). In recent years, there has been growing interest among higher education institutions in integrating cutting-edge quantum science experiments into the undergraduate curriculum (Rozenman et al., 2022). This shift is driven by the increasing demand for scientists and engineers in the rapidly evolving job market, where advanced technologies, such as quantum computing, quantum communication, and quantum sensing, play a crucial role (Kundu et al., 2023a; Meyer et al., 2025). By incorporating hands-on quantum experiments, universities aim to equip students with the skills and knowledge needed to thrive in these emerging fields. This educational approach fosters a deeper understanding of quantum mechanics and its applications, preparing graduates for careers that rely on the principles of quantum science and engineering, while also addressing the growing need for a workforce proficient in next-generation technologies.

This study introduces an experimental setup designed specifically for undergraduate students, utilizing pulsed lasers to investigate key quantum phenomena such as polarization entanglement, Bell's inequality, and quantum state tomography. By combining pulsed lasers with cost-effective, readily available optical components, such as polarizing beam splitters, pulsed laser detectors, and wave plates, this setup provides a comprehensive and scalable solution for undergraduate labs. The system allows students to directly manipulate and measure quantum states, offering them hands-on experience in implementing complex quantum protocols. Furthermore, this approach enables students to explore the nuances of quantum mechanics, from the fundamental principles of superposition and entanglement to the technical challenges of quantum state verification.

Integrating both topics into the curriculum bridges theoretical quantum mechanics with experimental practice, fostering a deeper understanding of the field. This approach allows students to observe the predicted outcomes of quantum theory firsthand while also developing essential practical skills in precision optics and data analysis, which are crucial for future studies in quantum technologies.

1.1. Quantum tomography and Bell's inequality

Quantum tomography is the process of estimating the properties of quantum states through numerous measurements on different aspects of the system's state (Scully and Suhail Zubairy, 1999). In most cases, including this experiment, these measurements correspond to the reconstruction of the quantum state's density matrix (Toninelli et al., 2019). The density matrix, denoted as ρ, encapsulates all the statistical information about a quantum state and is formally defined as (Schleich, 2001):

$$\rho \equiv |\psi\rangle\langle\psi| \tag{1}$$

In this experiment, we will reconstruct the density matrix of a randomized pulsed laser given by:

$$\rho = \begin{pmatrix} P_{HH-HH} & P_{HV-HH} & P_{VH-HH} & P_{VV-HH} \\ P_{HH-HV} & P_{HV-HV} & P_{VH-HV} & P_{VV-HV} \\ P_{HH-VH} & P_{HV-VH} & P_{VH-VH} & P_{VV-VH} \\ P_{HH-VV} & P_{HV-VV} & P_{VH-VV} & P_{VV-VV} \end{pmatrix} \tag{2}$$

and will proceed to test Bell's inequality. The density matrix of an entangled state will reveal the same properties as that of entangled particles. In this experiment, we will focus on entangling polarization states and demonstrate this by measuring their density matrix and testing Bell's inequality.

Table 1
Definition of two polarization states of the emitted pulses from the pulsed laser. The angles refer to the half-wave (θ_{HWP}) plate in the source.

Bit	θ_{HWP}	Polarization state
0	0°	$\|V\rangle$
1	90°	$\|H\rangle$

1.2. The CHSH test: A practical implementation of Bell's theorem

In this experiment, we will use the CHSH test, one of the most effective methods for demonstrating Bell's theorem (Zhang et al., 2021). The test defines a correlation function $E(\alpha, \beta)$, which quantifies the correlation between the measurement outcomes of two detectors aligned at angles α and β. The correlation function is expressed as (Huang et al., 2013):

$$E(\alpha,\beta) = \frac{N(\alpha,\beta) + N(\alpha_\perp,\beta_\perp) - N(\alpha,\beta_\perp) - N(\alpha_\perp,\beta)}{N(\alpha,\beta) + N(\alpha_\perp,\beta_\perp) + N(\alpha,\beta_\perp) + N(\alpha_\perp,\beta)} \tag{3}$$

Here, α and β represent polarization angles, with $\alpha_\perp = \alpha + 90°$. The quantity $N(\alpha, \beta)$ corresponds to the number of detected light pulses for detectors measuring at angles α and β. The Bell parameter S is computed using four specific polarizer settings a, a', b, and b' as follows:

$$S = E(a,b) - E(a,b') + E(a',b) + E(a',b') \tag{4}$$

The inequality $|S| \leq 2$ must always hold (Bell and Gao, 2016). However, quantum mechanics predicts that certain entangled states can achieve values such that $|S^{(QM)}| > 2$. A violation of this inequality confirms the non-local nature of quantum mechanics and demonstrates the strength of quantum correlations beyond classical expectations.

2. Experimental

The source used is a pulsed laser that generates polarized photons according to the laser's angle. The laser pulse travels through a polarizer, which adjusts the intensity of the light according to Malus's law. Next, the pulse propagates through a half-wave plate $\frac{\lambda}{2}$ (λ being the wavelength), which rotates the polarization of the incident pulse by twice the plate's physical rotation angle. The selection between these two states is made randomly for each photon (see Table 1).

Our experimental setup employs a classical pulsed laser rather than a single-photon source. The polarization of each pulse is randomized, thereby simulating the behavior of single photons with varying polarization states while the optical phase is kept fixed. This configuration is suitable for advanced quantum experiments, including quantum tomography and Bell's test. While genuine quantum systems utilize single photons to ensure the no-cloning theorem (Bloom et al., 2022) and to

enable violations of Bell's inequality, our use of classical laser pulses serves as a practical and educational analogy.

Classical light can be intercepted without altering the transmitted states in the same way as single photons, potentially allowing eavesdropping without detection. However, by carefully randomizing the polarizations and employing the same sequence of operations as in true quantum systems, we replicate the protocol flow, enabling the study of quantum properties such as state reconstruction in tomography and the testing of quantum entanglement through Bell's inequalities, without the need for complex single-photon sources.

Both Alice and Bob use polarized beam splitters (PBS) to filter pulses based on their polarization. The PBS separates the incoming pulses into distinct paths according to their polarization states. These filtered beams are then directed to two detectors (Logitech C270), where the intensity of each beam is measured, as depicted in Figs. 1, 2.

2.1. Derivation of analogous entanglement with pulsed source

In this section, we derive the transition from classical optical pulses to a Bell-type quantum state, establishing the theoretical foundation that underpins the entanglement-like behavior observed in our system. We demonstrate that our experimental apparatus acts as a complete emulator of Bell states, reproducing the characteristic correlations and state structure expected from true entangled photon pairs. Moreover, we analytically predict the density matrix expected to be reconstructed from tomographic measurements, offering a quantitative benchmark for experimental verification.

2.1.1. Source preparation

The pulsed laser emits coherent states with randomized polarization:

- Each pulse is prepared in either $|V\rangle$ (vertical) or $|H\rangle$ (horizontal) with equal probability:

$$p(|V\rangle) = p(|H\rangle) = \frac{1}{2} \tag{5}$$

- The source therefore prepares the coherent super-position described by:

$$|\psi_1\rangle = \frac{1}{\sqrt{2}}(|H_{Alice}, H_{Bob}\rangle + |V_{Alice}, V_{Bob}\rangle) = \frac{1}{\sqrt{2}}(|H_A, H_B\rangle + |V_A, V_B\rangle) \tag{6}$$

2.1.2. Beam splitter transformation

For each pulse $|P^{(i)}\rangle$ (where $P^{(i)} \in \{V, H\}$), the 50:50 beam splitter creates two copies:

$$|P^{(i)}\rangle \to |P_A^{(i)}\rangle \otimes |P_B^{(i)}\rangle \tag{7}$$

where $|P_A^{(i)}\rangle$ and $|P_B^{(i)}\rangle$ are coherent states sent to Alice and Bob respectively.

2.1.3. Ensemble average over many pulses

For N pulses, the joint state becomes:

$$\rho_{\text{joint}} = \frac{1}{N}\sum_{i=1}^{N} |P_A^{(i)}\rangle\langle P_A^{(i)}| \otimes |P_B^{(i)}\rangle\langle P_B^{(i)}| \tag{8}$$

As $N \to \infty$, this converges to:

$$\rho_{\text{joint}} = \frac{1}{2}|V_A, V_B\rangle\langle V_A, V_B| + \frac{1}{2}|H_A, H_B\rangle\langle H_A, H_B| \tag{9}$$

2.2. Measurement in different bases

Quantum tomography requires measurements in multiple bases:

(a) H/V basis:.

$$P(P_A, P_B) = \begin{cases} \frac{1}{2} & \text{if } (P_A, P_B) = (H_A, H_B) \text{ or } (V_A, V_B), \\ 0 & \text{otherwise.} \end{cases} \tag{10}$$

(b) D/A basis:. (Diagonal/Anti-diagonal)

$$|D\rangle = \frac{1}{\sqrt{2}}(|H\rangle + |V\rangle), \quad |A\rangle = \frac{1}{\sqrt{2}}(|H\rangle - |V\rangle)$$
$$P(D_A, D_B) = P(A_A, A_B) = \frac{1}{4} \tag{11}$$

2.2.1. Reconstructed density matrix

The tomography algorithm reconstructs:

$$\rho_{\text{recon}} = \begin{pmatrix} 0.5 & 0 & 0 & 0.5 \\ 0 & 0 & 0 & 0 \\ 0 & 0 & 0 & 0 \\ 0.5 & 0 & 0 & 0.5 \end{pmatrix} \tag{12}$$

This matches the density matrix of the Bell state:

$$|\psi_1\rangle = \frac{1}{\sqrt{2}}(|H_A, H_B\rangle + |V_A, V_B\rangle) \tag{13}$$

since:

$$\rho_{\psi_1} = |\psi_1\rangle\langle\psi_1| = \frac{1}{2}\begin{pmatrix} 1 & 0 & 0 & 1 \\ 0 & 0 & 0 & 0 \\ 0 & 0 & 0 & 0 \\ 1 & 0 & 0 & 1 \end{pmatrix} \tag{14}$$

2.2.2. Physical interpretation

- The off-diagonal elements (ρ_{14}, ρ_{41}) emerge from phase-coherent correlations in rotated bases
- The reconstructed matrix is identical to ρ_{ψ_1} despite the classical nature of the source
- This demonstrates how quantum tomography interprets classical correlations as quantum coherence

2.3. Mathematical derivation: Classical emulation of Bell state $|\psi_2\rangle$

2.3.1. Modified experimental setup

To emulate $|\psi_2\rangle$, we add a 90° half-wave plate (HWP) to Bob's path:

- The HWP (number 2 in Fig. 1) rotates polarizations: $|V\rangle \leftrightarrow |H\rangle$
- Alice's path remains unchanged

2.3.2. Source preparation

The pulsed laser again prepares states with randomized polarization:

$$|\psi_2\rangle = \frac{1}{\sqrt{2}}(|V_{Alice}, H_{Bob}\rangle + |H_{Alice}, V_{Bob}\rangle) = \frac{1}{\sqrt{2}}(|V_A, H_B\rangle + |H_A, V_B\rangle) \tag{15}$$

2.3.3. Beam splitter and polarization rotation

For each pulse $|P^{(i)}\rangle$ ($P \in \{V, H\}$):

$$|P^{(i)}\rangle \to \begin{cases} |V_A\rangle \otimes |H_B\rangle & \text{if } P = V \\ |H_A\rangle \otimes |V_B\rangle & \text{if } P = H \end{cases} \tag{16}$$

2.3.4. Ensemble average over many pulses

For N pulses, the joint state becomes:

$$\rho_{\text{joint}} = \frac{1}{N}\sum_{i=1}^{N} |P_A^{(i)}\rangle\langle P_A^{(i)}| \otimes |P_B^{(i)}\rangle\langle P_B^{(i)}| \tag{17}$$

Converging to:

$$\rho_{\text{joint}} = \frac{1}{2}|V_A, H_B\rangle\langle V_A, H_B| + \frac{1}{2}|H_A, V_B\rangle\langle H_A, V_B| \tag{18}$$

2.3.5. Measurement in different bases

(a) H/V basis:.

$$P(P_A, P_B) = \begin{cases} \frac{1}{2} & \text{if } (P_A, P_B) = (V_A, H_B) \text{ or } (H_A, V_B), \\ 0 & \text{otherwise.} \end{cases} \tag{19}$$

(b) D/A basis:.

$$P(P_A, P_B) = \begin{cases} \frac{1}{4} & \text{if } (P_A, P_B) \in \{(D_A, A_B), (A_A, D_B)\}, \\ 0 & \text{otherwise.} \end{cases} \tag{20}$$

2.3.6. Reconstructed density matrix

Tomography yields:

$$\rho_{\text{recon}} = \begin{pmatrix} 0 & 0 & 0 & 0 \\ 0 & 0.5 & 0.5 & 0 \\ 0 & 0.5 & 0.5 & 0 \\ 0 & 0 & 0 & 0 \end{pmatrix} \tag{21}$$

Matching the true Bell state:

$$\rho_{\psi_2} = |\psi_2\rangle\langle\psi_2| = \frac{1}{2}\begin{pmatrix} 0 & 0 & 0 & 0 \\ 0 & 1 & 1 & 0 \\ 0 & 1 & 1 & 0 \\ 0 & 0 & 0 & 0 \end{pmatrix} \tag{22}$$

We note here that the relative phase between the horizontal and vertical components is ($\phi \equiv 0$). Hence, the reconstructed density matrix is strictly real, matching the ideal Bell-state form.

We also note that tomography used here in the H/V and D/A bases only; cross-basis settings are unnecessary because the phase is locked at $\phi = 0$.

2.4. Tomography measurement

In this section, we aim to measure two specific polarization states, as described by Eqs. (6) and (24).

Eq. (6) describes a scenario where both Alice and Bob register the same polarization as the one emitted by the laser. For instance, if the laser sends a vertical polarization (V), both Alice and Bob will also receive vertical polarization (V).

$$|\psi_1\rangle = \frac{1}{\sqrt{2}}(|H_{Alice}, H_{Bob}\rangle + |V_{Alice}, V_{Bob}\rangle) \tag{23}$$

Eq. (24) describes a configuration in which Bob has an additional half-wave plate positioned before his PBS, rotated to 90°. In this setup, when Alice receives a vertical polarization (V), Bob will receive a horizontal polarization (H).

$$|\psi_2\rangle = \frac{1}{\sqrt{2}}(|V_{Alice}, H_{Bob}\rangle + |H_{Alice}, V_{Bob}\rangle) \tag{24}$$

To achieve the second term in both equations, the laser pulse needs to be randomized. This randomization ensures that the laser can emulate a mixed polarization state, thereby allowing Alice and Bob to measure entangled states with the correct correlations, as required for quantum tomography and Bell's test experiments.

To further analyze the impact of different polarization states and the configuration of the measurement setup, we examine the probabilities associated with the detection of the pulses, as summarized in Table 2. This table details the expected intensity of the detected signals for each polarization state sent by the source, depending on the settings of the half-wave plate.

The pulses are captured by the detector at a rate of 30 frames per second. These pulses are subsequently analyzed using image processing techniques in MATLAB. Each captured image is examined to identify the region of interest, which is then integrated to calculate the total power of the pulse. A MATLAB code sample for this analysis is provided in the supplementary material.

2.5. Violation of Bell's inequality

Bell's inequality represents a mathematical constraint on the correlations observed in measurements of entangled quantum systems (Bell, 1964; Gisin and Bechmann-Pasquinucci, 1998). It is derived from the principles of local realism, which assert that the properties of physical systems are predetermined prior to measurement and that any correlations observed between distant systems result from preexisting shared information (Liang and Doherty, 2007; Mari et al., 2023).

In contrast, quantum mechanics accommodates the phenomenon of entanglement, where two or more particles become intrinsically linked, resulting in their properties being interdependent. The predictions of quantum mechanics, including those involving entanglement, can violate Bell's inequality, thereby demonstrating that the behavior of entangled systems cannot be adequately described by local realism (Gröblacher et al., 2007).

The violation of Bell's inequality serves as a crucial indicator of the non-classical nature of entangled quantum states, which is essential for ensuring the efficacy of security protocols, such as quantum key distribution (QKD). By observing violations of Bell's inequality, the authorized parties can be confident that their quantum communication is secure from eavesdropping. This guarantees the presence of genuine quantum correlations necessary for establishing a secure key against potential interception by unauthorized parties (Singh et al., 2021).

To calculate Bell's inequality, we need to evaluate Eq. (4). In our setup, we removed half of the cameras and replaced the PBS with polarizers (see Fig. 3). Alice's angle is designated as α and Bob's angle as β. The current configuration, shown in Fig. 4, illustrates this arrangement, where the polarizers positioned near the detectors allow us to perform correlation measurements between Alice's and Bob's detection outcomes.

To calculate $N(\alpha, \beta)$, we processed the recorded video data for each pair of angles α and β, which contained the intensity of the received signals. We plotted the signal intensity over time, as depicted in Fig. 6 and applied a threshold to filter out noise, ensuring that only significant peaks were counted. The value of $N(\alpha, \beta)$ was obtained by counting the number of peaks that exceeded this threshold, representing valid detection events for each angle pairing. These measurements formed the basis for evaluating the violation of Bell's inequality.

For each camera, an intensity threshold was established to differentiate between 0 and 1 bits, as depicted in Fig. 6 by horizontal black files labeled as 'Threshold'. This threshold indicated whether the polarization of the sent bit matched the measured basis. Subsequently, the probability of detecting a signal was calculated for each camera or detector. By combining these probabilities, state density matrices were constructed using Eq. (3), which describes the relationship between the measured intensities and the underlying quantum states.

3. Results

3.1. Quantum tomography measurement

The quantum tomography measurements successfully reconstructed the density matrices of the emitted polarization states. For the aligned configuration, the observed outcomes closely matched the theoretical expectations described in Eq. (6). Both Alice and Bob measured identical polarization states—horizontal (H) or vertical (V)—with probabilities nearing 50% for sequences of 50 pulses. These results, Fig. 5(d)–(f), validate the accurate preparation and measurement of polarization states, confirming the capability of the setup to emulate quantum state tomography effectively.

When Bob's half-wave plate (HWP) was rotated by 90°, the expected complementary behavior between Alice's and Bob's measurements was observed, consistent with Eq. (24). In this configuration, Alice measuring a vertical state $|V\rangle$ corresponded to Bob detecting horizontal polarization $|H\rangle$. The complementary results, Fig. 5 sub-figures (a)

Table 2
Table of polarization state probabilities for pulses sent by the source and measured by Alice and Bob. The second column shows the rotation angle of the half-wave plate (θ_{HWP}) in the sending unit, which determines the polarization state. The percentages represent the expected intensity of the photon detection at each of Alice's and Bob's detectors, relative to the total intensity of the light pulse.

Send state	θ_{HWP}	Base states	Alice		Bob	
			Detector $\|V\rangle$	Detector $\|H\rangle$	Detector $\|V\rangle$	Detector $\|H\rangle$
$\|V\rangle$	0°	$\|\psi_1\rangle$	50%	0%	0%	50%
$\|H\rangle$			0%	50%	50%	0%
$\|V\rangle$	90°	$\|\psi_2\rangle$	50%	0%	50%	0%
$\|H\rangle$			0%	50%	0%	50%

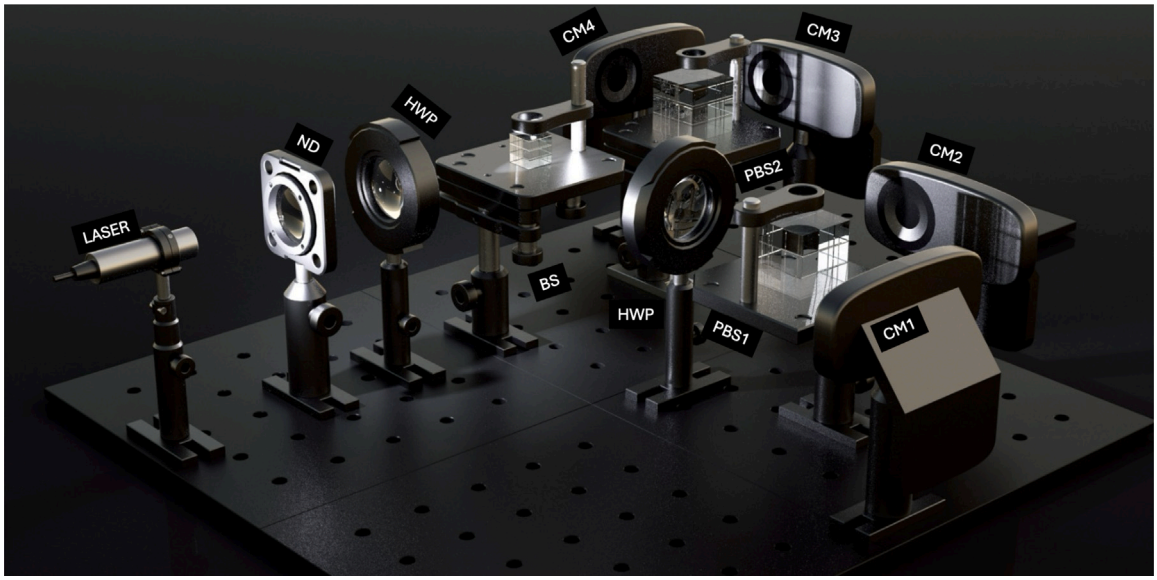

Fig. 1. Illustration of the experimental setup for the emulation of single-photon quantum systems using classical pulsed laser light. Each laser pulse is randomized in polarization to simulate the behavior of single photons with random polarization states, as required for quantum tomography. Alice and Bob use polarized beam splitters (PBS) to separate pulses based on polarization, directing the beams to two detectors for intensity measurement. Bob's half-wave plate is adjustable to control the polarization before detection, allowing the study of different polarization correlations, "BS" defines the 50:50 beam-splitter, "CM" defines the detector and "HWP" defines the half wave plate.

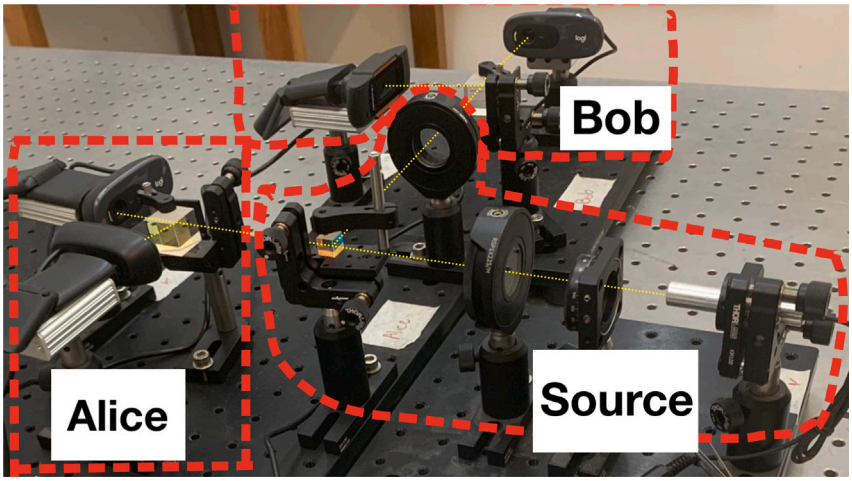

Fig. 2. Photo of the realistic experimental setup as depicted in Fig. 1. The yellow dashed lines represent the trajectories of the pulsed laser beams as they propagate through the system. These beams are polarized and directed towards beam splitters for separation based on polarization states. The red dashed lines highlight the key components of the system, including the source, Alice, and Bob. The source emits classical pulsed laser light, which is randomized in polarization to mimic single-photon behavior. Alice's and Bob's units include polarizing beam splitters (PBS) and detectors, with Bob having an additional adjustable half-wave plate to rotate the polarization before detection. The system's design is optimized to analyze the entangled states through randomized laser pulses, enabling the study of quantum-like behavior in a classical setup.

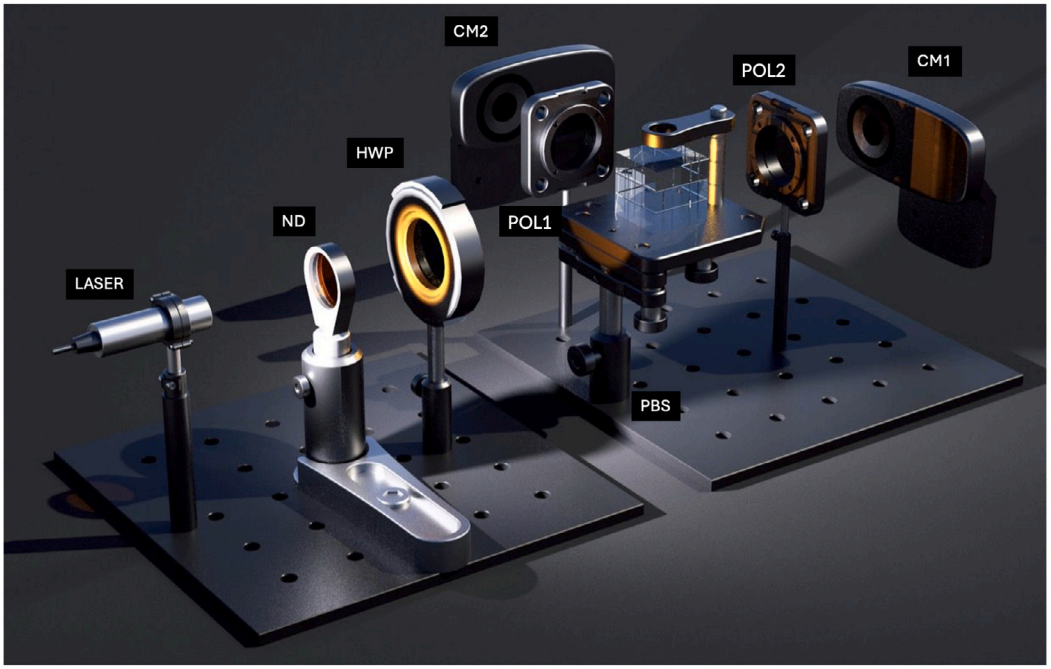

Fig. 3. Sketch of the experimental setup for testing Bell's inequality using entangled quantum systems. The setup consists of Alice and Bob, each equipped with polarizers at angles α and β, respectively. The laser is attenuated using a neutral density (ND) filter, and the pulse polarization is defined by a half-wave plate (HWP). The polarizers, placed next to the detectors, are used to perform Bell's test by measuring the correlations between Alice's and Bob's detection outcomes at various angle pairings, as detailed in Table 3. "CM" defines the detector and "PBS" defines the polarizing beam splitter.

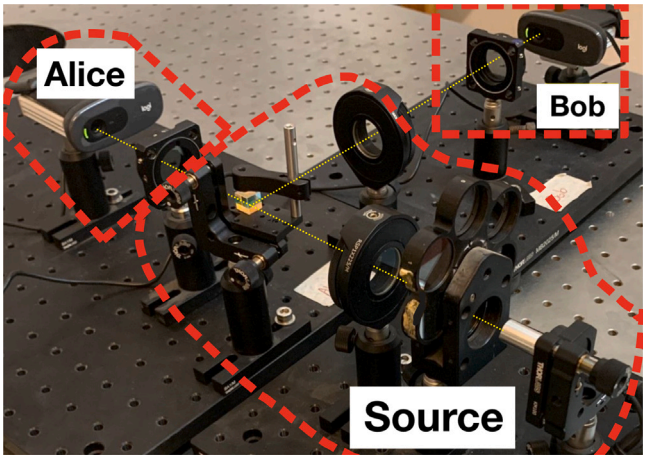

Fig. 4. Photo of the realistic experimental setup for testing Bell's inequality. The yellow dashed lines represent the paths of the attenuated laser pulses as they travel through the system. A neutral density (ND) filter is used to attenuate the laser, and the polarization of the pulses is controlled by a half-wave plate. Polarizers positioned near the detectors for both Alice and Bob, set at angles α and β, are used to measure polarization correlations. This setup is designed to evaluate the violation of Bell's inequality by analyzing detection outcomes for different angle pairings.

Table 3
The definition of the two polarization states of the pulsed laser. The angles correspond to the half-wave ($\lambda/2$) plate in the sending unit (Source).

α	β	N	α	β	N
−45°	−22.5°	12	45°	−22.5°	2
−45°	22.5°	2	45°	22.5°	11
−45°	67.5°	2	45°	67.5°	12
−45°	112.5°	11	45°	112.5°	2
0°	−22.5°	11	90°	−22.5°	2
0°	22.5°	10	90°	22.5°	2
0°	67.5°	2	90°	67.5°	10
0°	112.5°	2	90°	112.5°	11

to (c), correspond to the first bell state (6) and demonstrate that the system correctly measured correlations across different polarization bases, indicating proper alignment of all the optical elements and is in complete agreement with the theoretical prediction, as depicted in

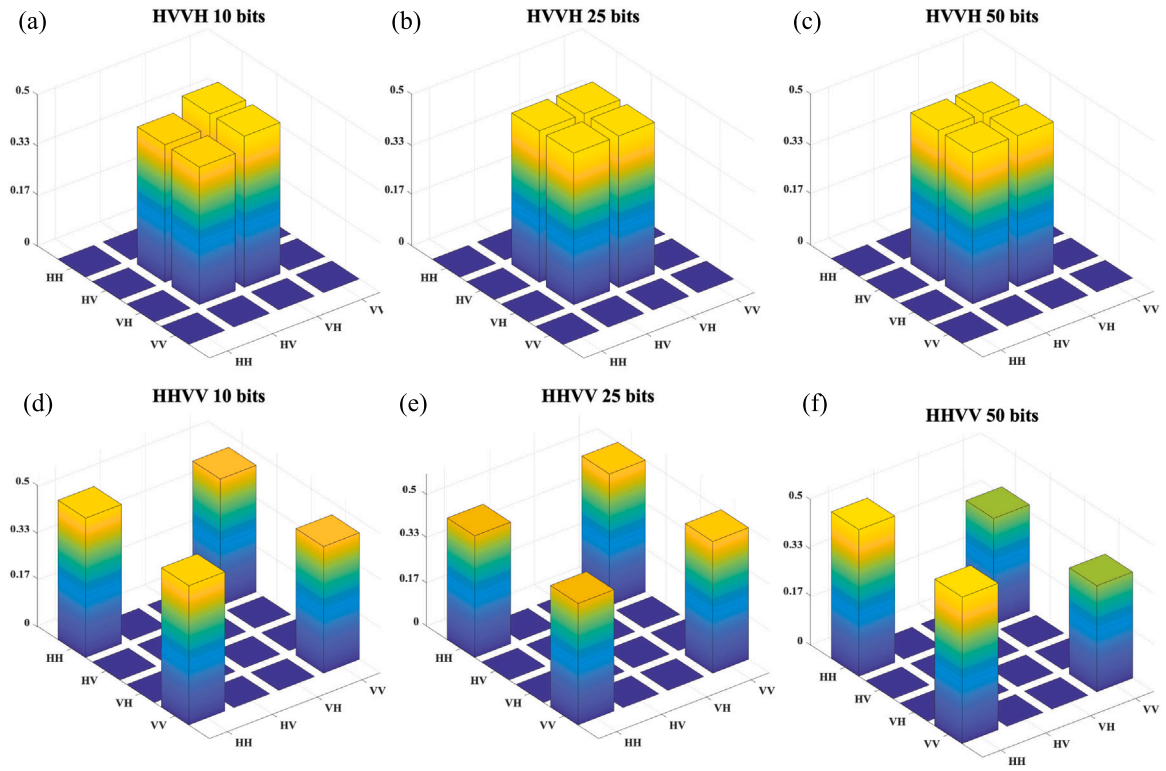

Fig. 5. Reconstructed density matrices from quantum tomography measurements results from quantum tomography measurements are shown as 3D column graphs, representing the reconstructed density matrices for two polarization states under analysis. Density matrices are presented for sequences of 10, 25, and 50 bits, highlighting the consistency and precision of the state reconstruction at varying data lengths. (a), (b), and (c) correspond to the aligned configuration, where Alice and Bob measure identical polarizations, as described by Eq. (5). (d), (e), and (f) depict the complementary configuration achieved by rotating Bob's half-wave plate by 90°, with correlations following Eq. (6). Column heights correspond to the magnitudes of matrix elements, capturing both probabilities and coherence between polarization states. The measurements demonstrate accurate quantum state reconstruction with minimal noise interference, confirming the setup's reliability in capturing polarization correlations.

Eq. (14). Subsequently, the results presented in Fig. 5, subfigures (d) to (f), demonstrate that our system successfully emulates the second Bell state, as defined in Eq. (24), and exhibits excellent agreement with the theoretical prediction shown in Eq. (22).

The tomography results highlight the effectiveness of this optical setup in reconstructing quantum-like density matrices. The precision in reproducing the polarization correlations shows that experimental noise, though present, had a minimal impact on the data quality. The reconstructed matrices reflect both the entanglement characteristics and statistical behavior required for accurate quantum state tomography, providing strong evidence of the system's reliability.

3.2. Violation of Bell's inequality

Using the CHSH test, we calculated Bell parameter S to assess the correlations between the polarization measurements. The experimental setup involved rotating Alice's and Bob's polarizers to specific angle pairs, α and β, respectively, as defined in Table 3. The resulting measurements were analyzed to determine the correlation function $E(\alpha, \beta)$ for each angle combination.

Our experiment yielded a Bell parameter of $S = 2.77$. This value significantly exceeds the classical limit of $S \leq 2$, providing clear evidence of quantum-like correlations between the polarization states. The successful violation of Bell's inequality demonstrates the presence of strong correlations that surpass the limits imposed by classical physics.

The signal intensity data for each α, β angle pair is shown in the subplots of Fig. 6. These subplots illustrate the peaks in detection events for various polarization settings, confirming the robustness of the measurement process. The high signal-to-noise ratio achieved in this experiment ensured reliable data collection, minimizing the effect of environmental disturbances.

4. Discussion

The successful quantum tomography measurements and Bell parameter $S = 2.77$ underscore the reliability and precision of the optical setup. The experiment provides a comprehensive demonstration of key quantum principles – such as state reconstruction and entanglement – through accessible and cost-effective tools.

4.1. Tomography accuracy and setup reliability

The quantum tomography results highlight the precision of the reconstructed density matrices. The close alignment between measured and expected outcomes suggests that the optical components – such as the polarizing beam splitters (PBS) and half-wave plates – were well-calibrated and properly aligned. Minor deviations from theoretical values were likely due to small a misalignment or environmental noise, which can affect pulse detection. Nonetheless, the system achieved robust state reconstruction, demonstrating that with proper calibration, undergraduate laboratories can explore advanced quantum concepts. Future improvements could involve automating the alignment process to reduce potential human error and integrating higher-sensitivity detectors. These enhancements would further increase the accuracy of density matrix reconstruction, making the setup suitable for even more precise experiments. In addition, incorporating advanced free-space optical communication techniques (Savino et al., 2024) could enhance educational setups for quantum state tomography and Bell's theorem experiments. Utilizing polarization for data transmission can provide students hands-on experience with quantum communication protocols, reinforcing theoretical principles in a practical context.

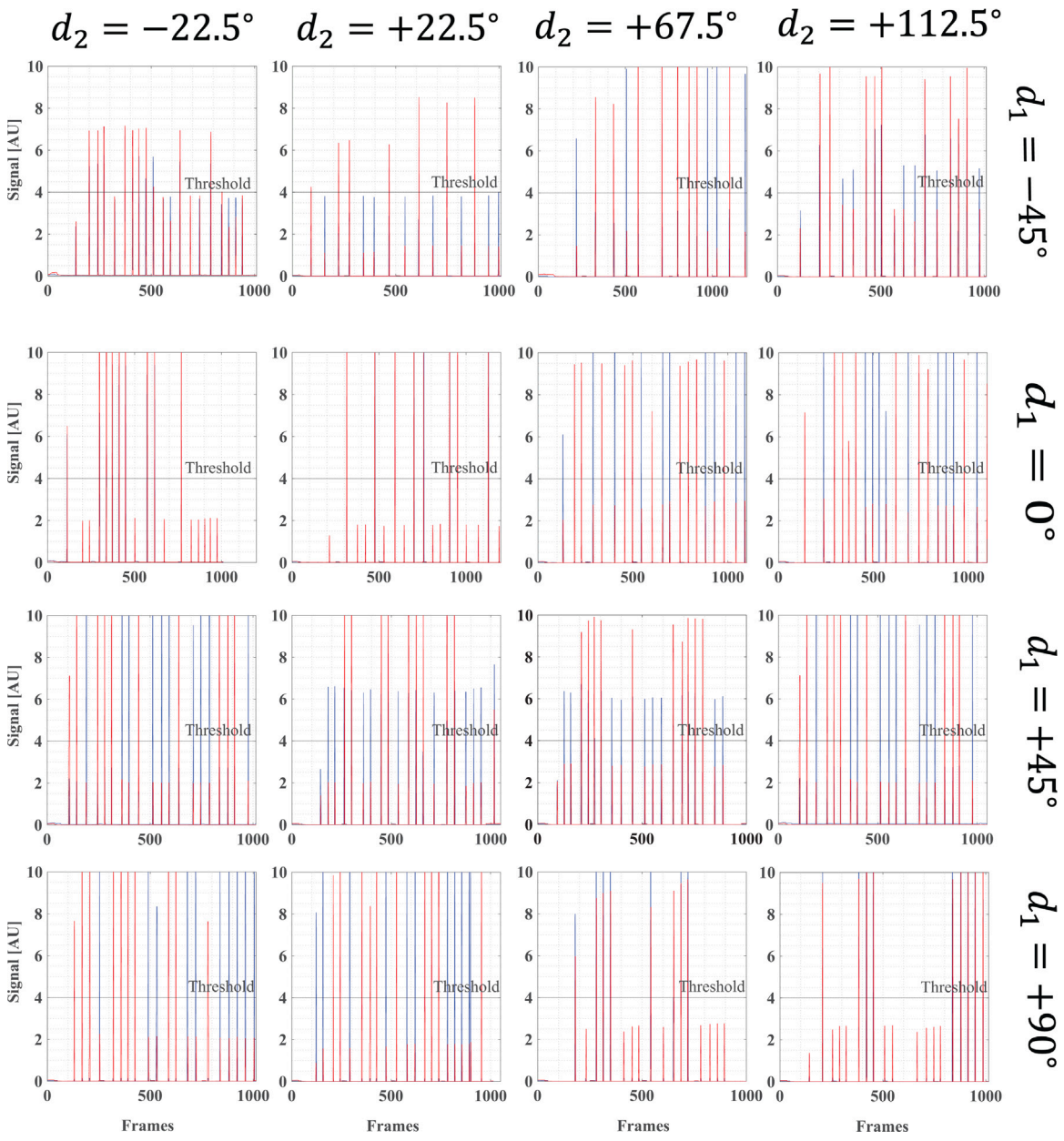

Fig. 6. Signal intensity data for Bell test measurements. The subplots display the signal intensity data for various polarization angle pairs (α, β), highlighting the peaks in measured intensities over time. A threshold filter is applied to exclude noise, ensuring only valid detection events are counted. These results are used to calculate the Bell parameter S, which exceeds the classical limit $S \leq 2$, with an experimental value of $S = 2.77$. This violation of Bell's inequality demonstrates quantum-like correlations between measurement outcomes.

4.1.1. Implications of Bell's parameter violation

The Bell parameter $S = 2.77$ indicates strong correlations between the polarization states, validating the use of classical laser pulses to emulate quantum-like behavior. The clear violation of Bell's inequality demonstrates that the optical setup was able to accurately capture non-classical correlations between the measurement outcomes. This outcome reinforces the practical utility of such experimental setups in teaching advanced quantum concepts, such as entanglement and quantum state verification.

4.1.2. Educational impact and practical considerations

This experiment provides an excellent platform for undergraduate students to explore complex quantum phenomena. By engaging with concepts such as quantum tomography and Bell's inequality violation, students gain hands-on experience with state-of-the-art quantum techniques. The simplicity and accessibility of the setup make it ideal for academic settings, where students can replicate foundational quantum experiments without the need for complex single-photon sources or specialized equipment. Future iterations of the experiment could explore additional quantum protocols, such as superposition states or quantum key distribution principles. These extensions would further enhance the educational value of the setup, preparing students for research and careers in quantum science and engineering.

4.1.3. Path forward for emulation experiments

The results of this experiment demonstrate the feasibility of conducting sophisticated quantum measurements using straightforward optical tools. However, the addition of more advanced components – such as automated polarization controllers or ultra-sensitive cameras

– could enhance the precision and scope of the experiments. These improvements would allow for even deeper exploration of quantum state properties and correlations, paving the way for more complex quantum experiments at the undergraduate level.

In summary, the experiment successfully reconstructed quantum-like density matrices and demonstrated a clear violation of Bell's inequality. The results confirm the capability of the optical setup to emulate key quantum behaviors, providing students with invaluable experience in quantum state measurement and analysis. With further refinements, this platform has the potential to become a cornerstone in the teaching of quantum mechanics, bridging the gap between theoretical concepts and practical experimentation.

The methodology introduced in this work is not limited to the optical domain but demonstrates significant potential for application across a broad spectrum of physical systems where classical hydrodynamics can emulate quantum mechanical behavior. Specifically, hydrodynamic analogs offer a tangible and intuitive platform to investigate features typically associated with matter-wave dynamics in quantum mechanics (Rodrigues Gonçalves et al., 2022). By leveraging this correspondence, our approach contributes to the expanding landscape of quantum–classical analogies, in which classical systems are employed to emulate, visualize, and gain insight into non-classical phenomena such as superposition, interference, and trajectory-based interpretations of quantum dynamics (Rozenman et al., 2023b, 2024; Weisman et al., 2021; Rozenman et al., 2023a).

CRediT authorship contribution statement

Eden Arbel: Writing – original draft, Software, Formal analysis, Data curation. **Noa Israel:** Writing – original draft, Software, Methodology, Data curation. **Michal Belgorodsky:** Writing – original draft, Data curation. **Yonathan Shafrir:** Writing – original draft, Data curation. **Alona Maslennikov:** Writing – review & editing, Conceptualization. **Sara P. Gandelman:** Writing – review & editing, Writing – original draft, Software, Conceptualization. **Georgi Gary Rozenman:** Writing – review & editing, Writing – original draft, Project administration, Methodology, Investigation, Formal analysis, Conceptualization.

Declaration of competing interest

The authors declare that they have no known competing financial interests or personal relationships that could have appeared to influence the work reported in this paper.

Acknowledgments

The authors would like to acknowledge the funding from the Committee for Budgeting & Planning of the Israel Council of Higher Education for their generous support in advancing Quantum Science and Technology (QST) in Tel Aviv University's advanced Physics laboratories.

Appendix A. Supplementary data

Supplementary material related to this article can be found online at https://doi.org/10.1016/j.rio.2025.100847.

Data availability

Data will be made available on request.

References

Bell, J.S., 1964. Phys. (Long Island City, N.Y.) 1, 195.
Bell, M., Gao, S. (Eds.), 2016. Quantum Nonlocality and Reality: 50 Years of Bell's Theorem. Cambridge University Press.
Bloom, Y., et al., 2022. Quantum cryptography—A simplified undergraduate experiment and simulation. Physics 4 (1), 104–123.
Rey-de Castro, R., Cabrera, R., Bondar, D.I., Rabitz, H., 2013. Time-resolved quantum process tomography using Hamiltonian-encoding and observable-decoding. New J. Phys. 15, 025032.
Doplicher, S., 2010. The principle of locality: Effectiveness, fate, and challenges. J. Math. Phys. 51 (1).
Einstein, A., Podolsky, B., Rosen, N., 1935. Phys. Rev. 47, 777.
Gandelman, S.P., Maslennikov, A., Rozenman, G.G., 2025. Hands-on quantum cryptography: Experimentation with the B92 protocol using pulsed lasers. Photonics 12 (3), MDPI.
Gebhart, V., Borgnia, E.A., Zhang, E.J., Chertkov, E., Wang, Z., Kondor, R., Claussen, N., 2023. Learning quantum systems. Nat. Rev. Phys. 5, 141–156.
Gisin, N., Bechmann-Pasquinucci, H., 1998. Bell inequality, Bell states and maximally entangled states for n qubits. Phys. Lett. A 246, 1–6.
Gröblacher, S., Paterek, T., Kaltenbaek, R., Brukner, Č., Żukowski, M., Aspelmeyer, M., Zeilinger, A., 2007. An experimental test of non-local realism. Nature 446, 871–875.
Huang, H.-L., Sun, Z.-Y., Wang, B., 2013. Bell–CHSH function approach to quantum phase transitions in matrix product systems. Eur. Phys. J. B 86, 1–7.
Kundu, N.K., McKay, M.R., Balaji, B., 2023a. Quantum enhanced sensing using Gaussian quantum states. In: Proceedings of the 2023 IEEE Sensors Applications Symposium. SAS, IEEE.
Kundu, N.K., Singh, A., Shukla, A.K., Srivastava, R., 2023b. Intelligent reflecting surface-assisted free space optical quantum communications. IEEE Trans. Wirel. Commun..
Liang, Y.-C., Doherty, A.C., 2007. Bounds on quantum correlations in Bell-inequality experiments. Phys. Rev. A 75, 042103.
Lib, O., Sulimany, K., Bromberg, Y., 2022. Processing entangled photons in high dimensions with a programmable light converter. Phys. Rev. Appl. 18, 014063.
Liu, R., et al., 2022. Towards the industrialisation of quantum key distribution in communication networks: A short survey. IET Quantum Commun. 3 (3), 151–163.
Mari, Luca, Wilson, Mark, Maul, Andrew, 2023. Measurement Across the Sciences: Developing a Shared Concept System for Measurement. Springer Nature.
Meyer, J., et al., 2025. Analogy of free-space quantum key distribution using spatial modes of light: scaling up the distance and the dimensionality. Opt. Lett. 50 (10), 3297–3300.
Nadlinger, D.P., Drmota, P., Nichol, B.C., Araneda, G., Main, D., Srinivas, R., et al., 2022. Experimental quantum key distribution certified by Bell's theorem. Nature 607, 682–686. http://dx.doi.org/10.1038/s41586-022-04891-2.
Paraïso, T.K., et al., 2021. Advanced laser technology for quantum communications (tutorial review). Adv. Quantum Technol. 4 (10), 2100062.
Parakh, A., et al., 2020. Quantum cryptography exercise schedules with concept dependencies. J. Colloq. Inf. Syst. Secur. Educ. 8 (1).
Pospiech, G., 2021. Quantum cryptography as an approach for teaching quantum physics. In: Teaching-Learning Contemporary Physics: From Research To Practice. pp. 19–31.
Rodrigues Gonçalves, M., et al., 2022. Bright and dark diffractive focusing. Appl. Phys. B 128, 51.
Rozenman, G.G., Peisakhov, A., Zadok, N., 2022. Dispersion of organic exciton polaritons—A novel undergraduate experiment. Eur. J. Phys. 43, 035301.
Rozenman, G.G., et al., 2023a. Bohmian mechanics of the three-slit experiment in the linear potential. Eur. Phys. J. Spec. Top. 232, 3295–3301.
Rozenman, G.G., et al., 2023b. Observation of Bohm trajectories and quantum potentials of classical waves. Phys. Scr. 98, 044004.
Rozenman, G.G., et al., 2023c. The quantum internet: A synergy of quantum information technologies and 6G networks. IET Quantum Commun. 4 (4), 147–166.
Rozenman, G.G., et al., 2024. Observation of a phase space horizon with surface gravity water waves. Commun. Phys. 7, 165.
Savino, N., et al., 2024. Robust free-space optical communication utilizing polarization for the advancement of quantum communication. Entropy 26, 309.
Schleich, W.P., 2001. Quantum Optics in Phase Space. John Wiley & Sons.
Scully, Marlan O., Suhail Zubairy, M., 1999. Quantum Opt. 648.
Singh, J., Ghosh, S., Arvind, Goyal, S.K., 2021. Role of Bell–CHSH violation and local filtering in quantum key distribution. Phys. Lett. A 392.
Stricker, R., Meth, M., Ahrens, J., Bohmann, M., Silberhorn, C., 2022. Experimental single-setting quantum state tomography. PRX Quantum 3, 040310.
Sulimany, K., Bromberg, Y., 2022. All-fiber source and sorter for multimode correlated photons. Npj Quantum Inf. 8, 4. http://dx.doi.org/10.1038/s41534-021-00515-x.
Sulimany, K., Vadlamani, S.K., Hamerly, R., Iyengar, P., Englund, D., 2024. Quantum-secure multiparty deep learning. arXiv preprint arXiv:2408.05629/.
Toninelli, E., Ndagano, B., Vallés, A., Nape, I., Rosales-Guzmán, C., Sephton, B., Forbes, A., 2019. Concepts in quantum state tomography and classical implementation with intense light: a tutorial. Adv. Opt. Photonics 11, 67–134.
Wang, J., et al., 2020. Scalable quantum tomography with fidelity estimation. Phys. Rev. A 101 (3), 032321.
Weisman, D., et al., 2021. Diffractive guiding of waves by a periodic array of slits. Phys. Rev. Lett. 127, 014303.
Zhang, W., Saripalli, R.K., Leamer, J.M., Glasser, R.T., Bondar, D.I., 2021. Experimental violation of the Leggett-Garg inequality using the polarization of classical light. Phys. Rev. A 104, 043711.